PAPER TODO LIST

Literature review [all]

- ☐ (would be good but not essential) Fig 7 add one or two more points per case
- ☐ (essential) 8 Add a couple more TKE cases to the plot (hopefully find a trend)
- ☐ Figure 4 (right): could we redo this Cd calculation and check if the results match if we add the base drag and viscous forces? If the results are still off, we should probably try to better explain
- ☐ we should flip Figs 9 so the order is consistent with the previous figures.
- ☐ (essential) We want to remove/replace Fig 10. Instead, we was want to simulate a case at either 4 or 10 deg AOA using the the transitional RANS model and compare against Fig 7 (this would only give us one Magnus force per AOA). If this is simple, we can modify the freestream TKE levels to assess the effect on the transitional model.

Boundary layer state on the Magnus force prediction for spin-stabilized projectiles

Duosi Fan *, Aaron Grenke †
University of Waterloo, Waterloo, Ontario, Canada

Xioahua Wu ‡
Royal Military College of Canada, Kingston, Ontario, Canada

Jean-Pierre Hickey §
University of Waterloo, Waterloo, Ontario, Canada

The accurate estimation of the Magnus force, and resulting moments, is needed for guidance, control, and navigation of spin-stabilized projectiles. The small magnitude of this force relative to other components renders the estimation of Magnus effects more susceptible to experimental and numerical uncertainties. The boundary layer characteristics are shown to play a first-order role in the prediction of this side force. As a result the numerical modelling assumptions, particularly related to the boundary layer transition, development and growth, can drastically influence the Magnus force estimate. Starting from experimentally-validated baseline cases, we conduct systematic computational fluid dynamic simulations using NASA's CFLD3D code with standard Reynolds-Averaged Navier-Stokes turbulence closure models and show the significant impact of the location of the transition on the Magnus force estimation. The magnitude

*Ph.D. student, Department of Mechanical and Mechatronics Engineering, 200 University Ave W.
†Undergraduate student, Department of Mechanical and Mechatronics Engineering, 200 University Ave W.
‡Professor, Department of Mechanical and Aerospace Engineering, and AIAA Associate Fellow.
§Assistant Professor, Department of Mechanical and Mechatronics Engineering, 200 University Ave W.

of the Magnus force coefficient is reduced by delaying transition to turbulence on the spin-stabilized projectile. Other numerical parameters such as the freestream turbulence, selection of the thermal boundary conditions or turbulence model play a lesser role. Given the strong dependence on transition location, we assess the use of transitional turbulence models for the prediction of aerodynamic coefficients. These present results underline the importance of numerical modelling parameters in the estimation of the Magnus force and moment for spin-stabilized projectiles.

Nomenclature

Ω = Dimensionless spin rate

C_D = Axial force coefficient

C_N = Normal force coefficient

C_y = Magnus/side force coefficient

P = Spin rate (rad/s)

$\vec{V}$ = Free-stream velocity (ms^{-1})

D = Model base diameter (m)

L = Model length (m)

α = Attack angle ($^\circ$)

TKE = Turbulent kinetic energy intensity (m^2s^{-2})

γ = intermittency factor

I. Introduction

The stability of a rocket or a projectile is greatly improved by the addition of a controlled spin. Spin-stabilized devices use the gyroscopic effects to overcome slight eccentricities in the aerodynamic forces and simplify the control. However, the rotation also generates flow asymmetries which can cause unintended side forces to the vehicle. A slight side force can result in a yaw motion which leads to a misalignment between the roll and velocity vectors; a misalignment which further accentuates the deviation due to a Magnus force directed perpendicular to the cross product of the effective velocity and rotation. The Magnus force, and the resulting Magnus moment, are caused to a great extent by an unequal pressure distribution on the port and starboard sides of the projectile as the axis of rotation and the flow velocity vector are not aligned. Although small, this force and moment represent a non-damped contribution which needs to be characterized for precise control, navigation, and guidance.

For the design of classical non-rotating projectiles, the stability derivatives can be estimated either by an empirically-defined, low-order model, using modified vortex panel methods or through steady-state Computational Fluid Dynamic (CFD) solvers. The calculation of these statically-stable projectile configurations have been well-established and the available tools provide robust and accurate estimates (see e.g. [1]). However, due to the complex flight dynamics, the estimation of stability derivatives in spin-stabilized projectiles present additional challenges. In spin-stabilized devices, an aerodynamic asymmetry is more difficult to quantify through simple low-order models (although low-order models may still be insightful for simplified geometries) and interference due to canards or fins can greatly influences the estimation of the Magnus force [2]. This difficulty is further compounded by the strong non-linearities in the stability derivatives due to the Magnus effect. In the transonic regime, the predictive challenges become even more severe as the

conning frequency varies significantly [3], a motion which can be further accentuated by the highly nonlinear Magnus moments [4]. Thus, the accurate quantification of the Magnus effects becomes critical for control and guidance of spin-stabilized devices.

Testing at in-flight conditions is undoubtedly the most accurate means to estimate the stability derivatives including the Magnus force and moment [5]. But it is clear that these tests imply high costs and significant experimental uncertainty. Therefore, most design work relies on a combination of sub-scale wind tunnel experiments and predictive modelling. Due to their highly non-linear and undamped behaviour, the Magnus forces cannot be neglected in spinning projectiles yet their contribution to the overall dynamics of the vehicle remains relatively small (between 1/100 and 1/10 of the normal force [6]). It is clear the experimental and modelling uncertainties must be smaller in magnitude than the Magnus force and moments estimates. Since the 1950s, there have been continual efforts to characterize the Magnus force and moments for spin-stabilized devices; among these initial experiments, we note the work by [6–10]. The objective of these works were two-fold: first, they sought to quantify the Magnus force given a set of flight parameters; second, and most importantly, they sought simplified three-dimensional boundary layer models to predict the Magnus force and moment. The elegance and simplicity of these physics-based predictive models have been, to some extent, slowly replaced by higher-fidelity numerical computations. Some of the more recent experimental works have focused on empirical modelling of the Magnus forces based on experimental measurements. For example, Oh *et al.* [5] proposed a framework to study spinning projectiles and developed simple regression models to reduce the state space and quantify the resulting uncertainty.

Increasingly, the trend is towards the use of predictive modelling using high-fidelity flow solvers to compute the damping coefficients and Magnus moments. The start of this trend can be traced back to the early numerical works by Nietubicz *et al.* [11]. Although generally more accurate than low-order models, Computational Fluid Dynamics (CFD) of turbulent flows with a rotating projectile rely on a number of modelling assumptions that increases the modelling uncertainty of these computational tools. DeSpirito and Silton [12] noted that both Reynolds Averaged Navier Stokes (RANS) and Large Eddy Simulations (LES) provide a similar level of accuracy for the computation of the Magnus moments. However, when the Mach number was in the transonic or low supersonic regime, higher-fidelity computational methods are required for better predictions [13]. In these regimes, hybrid RANS/LES has been shown to improve predictions but comes with about an one order of magnitude increase in computational cost compared to RANS alone [14]. Similarly, a better trajectory prediction was obtained using a Detached Eddy model which assumes a near wall RANS model [15]. Given the strong interaction between various components of the projectile during maneuvering, steady-state simulations are not able to capture the entire physics and unsteady simulations are often needed [13]. Bhagwandin [16] showed very good agreement between unsteady CFD simulations and experimental data. However, the accuracy of the predictions decreased as the angle of attack increased. This suggests that modelling of the separated flow on these rotating devices greatly impacts the prediction capabilities. The work by Doraiswamy *et al.* [15]

further showed the sensitivity of the trajectory prediction–and more specifically related effects due to the Magnus force computation–to the turbulence modelling. Based on the evidence of these previous studies, one can easily conclude that the Magnus force estimates are sensitive to the numerical modelling assumptions. The present work seeks to understand and quantify the sensitivity of some of these modelling assumptions on the Magnus force estimations for spin-stabilized devices.

The three main contributions to the Magnus force are [17]: the circumferential skin friction, centrifugal pressure and pressure due to the asymmetrical displacement thickness. These parameters depend heavily on the boundary layer state and evolution as shown earlier by [9]. The fluid dynamic aspects of the boundary layer flow require a more rigorous consideration to understand and quantify uncertainty on the Magnus force prediction. This is particularly true for the transition to turbulence on these rotating devices. In fact, for a canonical rotating cylinder in crossflow, the asymmetric transition between the top and bottom of the cylinder–and the resulting discrepancy in the flow separation regions– can generate an inverse Magnus force under certain very specific conditions [18, 19]. In other words, the resulting changes of the transition location leads to a force acting in the opposite direction of the classically predicted Magnus force in a rotating cylinder in crossflow [18, 19]. This is clear evidence that the boundary layer state can play a significant role on the flow separation and concomitantly on the dynamics of these rotating system. The effects of differing transition locations are not as important for rotating projectile–primarily due to the shallow angle between the flow and rotation vectors–but, due to the strong nonlinear behaviour which characterize these flows, can lead incorrect Magnus force estimates. From a modelling perspective the asymmetric distortion to the boundary–especially with regards to transition–remains very challenging to quantify given the three-dimensional nature of the boundary layer flow. Analytical works have considered the transition on a rotating cone with perfectly incident flow [20, 21]. More recent works have considered the effect of transition on an abstracted spinning cone [22]. Other works have applied transitional models to rotating projectiles with some success [2]. From an experimental perspective the quantification of the three-dimensionality boundary layer is also a challenge. Very recent works have proposed the use of Magnetic Resonance Velocimetry (MRV) to compute all three velocity components on a rotating projectile [23].

The boundary layer transition on a spin stabilized projectile is a function a number of independent parameters. In these flows, the transition is induced by crossflow instabilities as a result of the three-dimensional nature of the boundary layer. For non-rotating projectiles, the level of freestream perturbations will dictate if the mechanism of boundary layer transition is caused by spanwise aligned Tollmien-Schlichting wave (at low freestream turbulence intensity) or any number of the reported bypass transition mechanism in wall bounded flows (at higher freestream turbulence intensity). The importance of the freestream turbulence intensity with respect to crossflow instabilities remains unclear. As reported in [22], most predictive simulations for Magnus force calculations do not account for transitional models and assumes the boundary layer to be fully turbulent. Furthermore, most transitional models used in RANS-based simulations, such as $\gamma - Re_\theta$ [24] are based on correlation coefficients and are thus ill-suited for crossflow dominated transition [25]. A

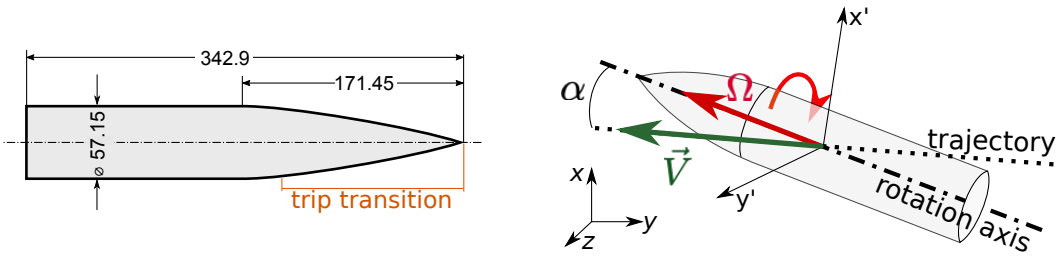

Fig. 1 Geometry of the rotating projectile in millimeters (left). The conical tip has a radius of 1079 mm from origin located at 262 mm from the tip (along the centerline axis) and 1046.7 mm in the perpendicular direction. Global and local coordinate system of the rotating projectile (right).

number of recent works have proposed models to account for the crossflow [25–27] but remain primarily focused on fixed-wing aerospace applications.

In this work, we seek to quantify the importance of the modelling parameters in the estimation of the Magnus force on a rotating projectile. More specifically, we quantify the uncertainty related to the boundary layer transition location with respect to the simulation parameter space. In Section II, the theoretical basis for the estimation of aerodynamic forces and moments is presented along with the a summary of the physical principles behind the Magnus force estimation. Section III describes the numerical setup of interests and details on the solver used. The results are validated and compared against experimental results in section IV. The results and conclusions are left for Sections V and VI.

II. Theoretical Background

We present the most important parameters and their corresponding nondimensionalization specifically for the characterization of the Magnus effect. We assume that the projectile is rotating about its body-fixed axis, x, at angular velocity of p. We can define a dimensionless spin rate, Ω, as:

$$\Omega = \frac{pD}{\left|\vec{V}\right|}, \tag{1}$$

where D and $\left|\vec{V}\right|$ are the projectile base diameter (in m) and the magnitude of the freestream velocity (in m/s), respectively; for notational simplicity, we will denote $\left|\vec{V}\right|$ as V in the following. The following additional quantities account for the forces in spin-stabilized configurations. The roll damping moment is:

$$\frac{1}{2}\rho V^2 SD\left(\frac{pD}{V}C_{l_p}\right), \tag{2}$$

where C_{l_p} is the roll damping moment coefficient. Here, S represents the characteristic area of the projectile. For simplicity, it is standard to use the spin-derivative coefficient only, such that: $C_{l_p} = \frac{\partial C_{l_t}}{\partial \Omega}$, where C_{l_t} is the total roll moment coefficient.

The Magnus force is proportional to the angle of attack, α, and is defined as:

$$\frac{1}{2}\rho V^2 SD\left(\frac{pD}{V}C_{Y_{p\alpha}}\right)\sin\alpha, \tag{3}$$

whereas the Magnus moment is:

$$\frac{1}{2}\rho V^2 SD\left(\frac{pD}{V}C_{n_{p\alpha}}\right)\sin\alpha. \tag{4}$$

Here, $C_{Y_{p\alpha}}$ is the Magnus force derivative coefficient and $C_{n_{p\alpha}}$ is the Magnus moment derivative coefficient. Again, for simplicity, we only compute the spin derivatives in these dynamic stability calculations:

$$C_{Y_p} = \frac{\partial C_Y}{\partial \omega}, \qquad C_{n_p} = \frac{\partial C_n}{\partial \omega}, \tag{5}$$

where C_Y and C_n represent the side force and yaw moment coefficients, respectively.

III. Numerical Parameters

The multi-block, compressible Reynolds Averaged Navier-Stokes (RANS) solver CFL3D [28], which was developed by NASA*, was used in the present investigation. The code represents a well-tested and validated steady and unsteady computational fluid dynamics solver used for external aerodynamic applications. The multi-block, structured grid solver benefits from a very high computational efficiency compared to unstructured codes. This computational efficiency is thus limited to the study of simple geometries; for more complex geometries, unstructured codes are often necessary. The solver discretizes the Euler flux via a classical Roe scheme and the MUSCL interpolation ensures the second-order spatial accuracy. The temporal discretization is achieved through an implicit approximate-factorization method. A more detailed description of the implementation, including the numerical schemes, can be found in [28]. The solver requires a structured mesh which results in a more complex grid generation process but it limits the discretization errors and provides a good control on the near wall resolution and wake regions of the spinning projectile. The optimal multi-block grid generation was achieved through the use of Pointwise meshing software.

For all wall resolved cases discussed herein, the first grid point was set to about y^+=1; this strict requirement was enforced at the wall boundaries through out the entire computational domain. The total number of grid points for the steady and unsteady simulations was just below 2×10^6. The grid stretching, in the wall normal direction, was limited to about 1.1 to assure accurate near-wall resolution and limit the discretization errors. The simulations were run in both a steady and unsteady state with appropriate freestream boundary conditions listed below. The domain size was assessed to assure that the imposed boundary treatment did not affect any of the domain of interest. We assured convergence in the steady cases by reducing, by at least 6 orders of magnitude, the residual of the variables of interest

*https://github.com/nasa/CFL3D

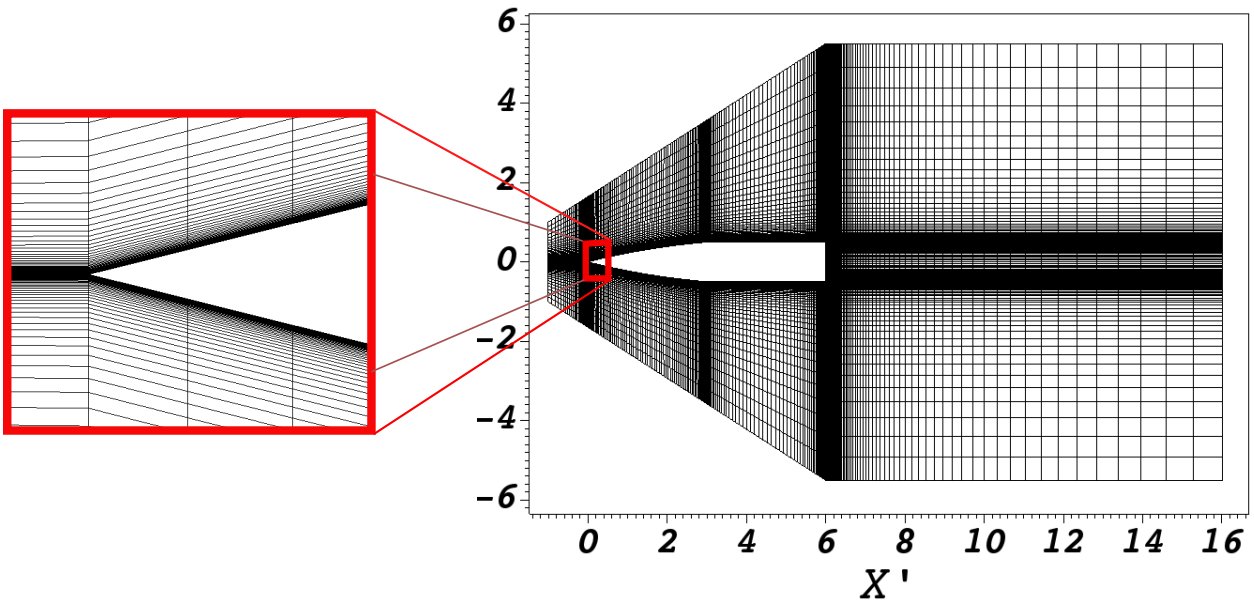

Fig. 2 Representative view of computational mesh and projectile. A close-up of the tip is shown.

for the computation. A multi-grid method, with a W profile, was used to accelerate the convergence of the steady simulations. This approach typically reduced the number of pseudotime steps on the finest mesh to achieve the desired convergence. For the unsteady cases, a physical time step, based on the CFL number, was set in order to capture the important physical processes required for the Magnus force calculation. The closure of the turbulence RANS equations is achieved using SST approach. We account for the turbulence effect on the mean flow by computing the evolution of the turbulence length scales through additional transport equations for the turbulent kinetic energy and specific dissipation. The turbulence equations are computed down to the wall without additional modelling assumption for our baseline simulations. Here the classical implementations of the turbulence models are used.

A. Laminar-to-turbulent transitional modelling

In classical RANS modelling, the contribution of the laminar boundary layer prior to transition is often of negligible importance; for most engineering purposes at sufficiently high Reynolds number, the boundary is implicitly assumed to be fully turbulent from the leading edge. Yet, at higher Mach numbers, compressibility acts to stabilize the viscous modes of boundary layer transition [29], thus physically delaying transition to turbulence. Furthermore, as a turbulent boundary layer remains more resilient to adverse pressure gradients, the state of the boundary layer has a large role in the extent of flow separation. As a result, the laminar-to-turbulent transition location plays a central role, both direct and indirect, for Magnus force prediction in spin-stabilized projectiles.

In this work, two approaches are used to modify the transition location. The first approach consists of an *a priori* defined transition location; this approach mirrors the transition strips used in most experiments reported in the literature.

Table 1 Summary of baseline validation cases.

Case	Variable	Ma	$\mathbf{Re_L} \times (10^{-6})$	Attack angle (α)	Spinning Rate	Ref.
I	Surface Pressure	3	6.39	4°,10°	0	[31]
II	Aerodynamic Coefficient	3	7.317	multiple	multiple	[32]
III	Boundary Layer	3	7.3	4.2°	0.19	[33]

We force the eddy viscosity to zero upstream of the pre-defined transition location; from the prescribed transition location onwards, the eddy viscosity evolves and is computed via the turbulence transport equations. The second approach consists of computing transition based on a classical correlation-type transitional model. In the present work, the $\gamma - Re_\theta$ model [30] is used; it represents the most prevalent transitional model in engineering-focused CFD codes. Additional transport equations for intermittency factor (γ) and, a slightly more heuristically defined, boundary layer Reynolds number (Re_θ) are solved during the simulation. The governing equation for intermittency is given by:

$$\frac{\partial(\rho\gamma)}{\partial t} + \frac{\partial(\rho U_j \gamma)}{\partial x_j} = P_\gamma - E_\gamma + \frac{\partial}{\partial x_j}\left[\left(\mu + \frac{\mu_t}{\sigma_f}\right)\frac{\partial \gamma}{\partial x_j}\right] \tag{6}$$

Although this transitional model is ubiquitous in transitional RANS modelling capturing bypass transition, it is not developed to account for crossflow induced transition prediction. We note that some correlation-based transitions have been developed to account for the crossflow instabilities [25]. The objective of the present work is to assess the existing transitional models and their effects on the Magnus force estimation.

IV. Comparative Baseline Simulations

Well-defined baseline simulations were first conducted in order to establish a set of experimentally validated cases covering a range of operating conditions in this study. These baseline simulations are validated using publicly available experimental data which focus on various measurements of aerodynamic forces including the Magnus force. All of these experimental tests were conducted at the Ballistic Research Laboratory (BLR) and reported in the open literature. The geometry of the generic projectile is shown in figure 1. This rotating projectile does not have any fins which simplifies the interpretation of the resulting side forces on the projectile. It is especially important in the present study where the boundary layer effects on the Magnus force and moments are considered. As such our objective is to isolate the boundary layer effects from other possible forces such as the interaction between body/fins in a more complex projectile geometry. A more realistic, finned geometry may be valuable for applied engineering design but the added aerodynamic complexity renders a focused analysis more difficult to study. The validation cases in the supersonic regime include the comparison of surface pressure [31], aerodynamic coefficient [32], and detailed boundary layer [33] data at various spinning rates (with those data from either static or spinning measurements). Table 1 summarizes the main characteristics of each computation with the corresponding published references.

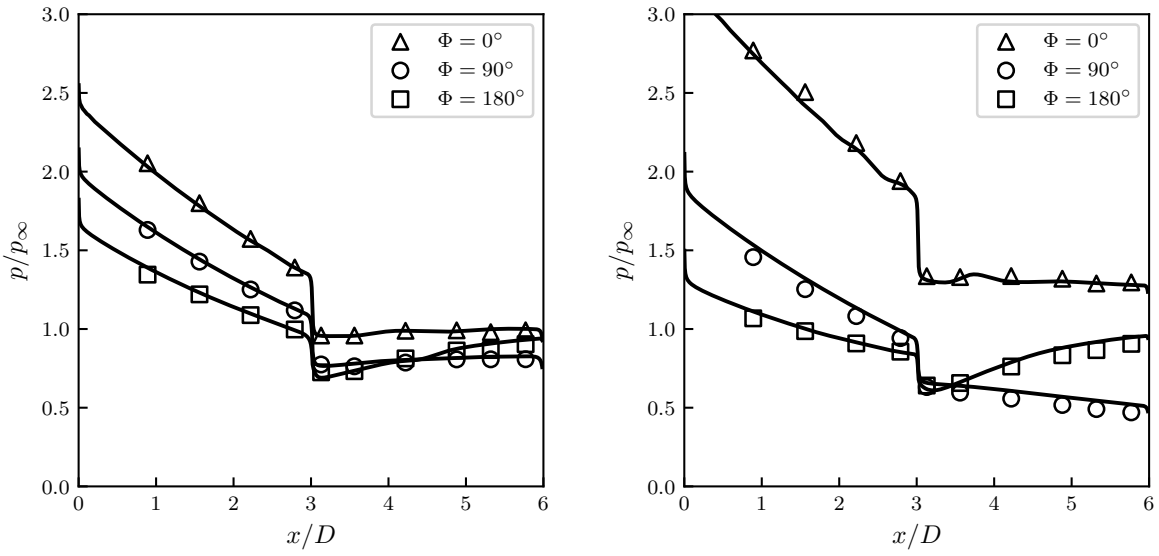

Fig. 3 Case I: Surface pressure distribution (line) at $\alpha = 4°$ (left) and $\alpha = 10°$ (right) compared with the experimental data (symbols) [31].

A. Pressure distribution validation

A first simulation is conducted without rotation to assess the pressure distribution about the projectile for various angles of attack (Case I). For the steady simulation, we use the standard mesh (with wall resolution) and modelling parameters as described in the previous subsection. All of the present comparative baseline cases are computed with a transition location fixed at $x/D = 0.722$, which corresponds to the trip wire position in the experiment. Figure 3 shows the pressure distribution on the body at various azimuthal locations on the projectile; two angles of attacks are considered: $\alpha = 4°$ and $10°$. A near perfect agreement with experimental results is noted for the pressure distribution about the projectile. The simulations capture the pressure drop, at the interface of the conical tip and the cylindrical body at $x/D = 3$. The accurate pressure distribution prediction without rotation is a necessary but insufficient condition for Magnus force on rotating bodies.

B. Aerodynamic coefficients validation

The Case II considers the same projectile, at the same freestream velocity but at various spin rates and over a range of angles of attack. The normal and drag force coefficients are computed without spinning which is consistent with the experiments. The computed aerodynamic coefficients are compared against the experimental results in figure 4; the definition of these coefficients can be found in Section 2. The normal force is well captured by the simulations over all the range of angles of attack while the drag force coefficient is under-predicted about 20% over the same range. The source of this discrepancy is uncertain but could be related to the additional drag component due to the experimental support structure in the experiment (or a non-linear interaction between the projectile and the support structure.

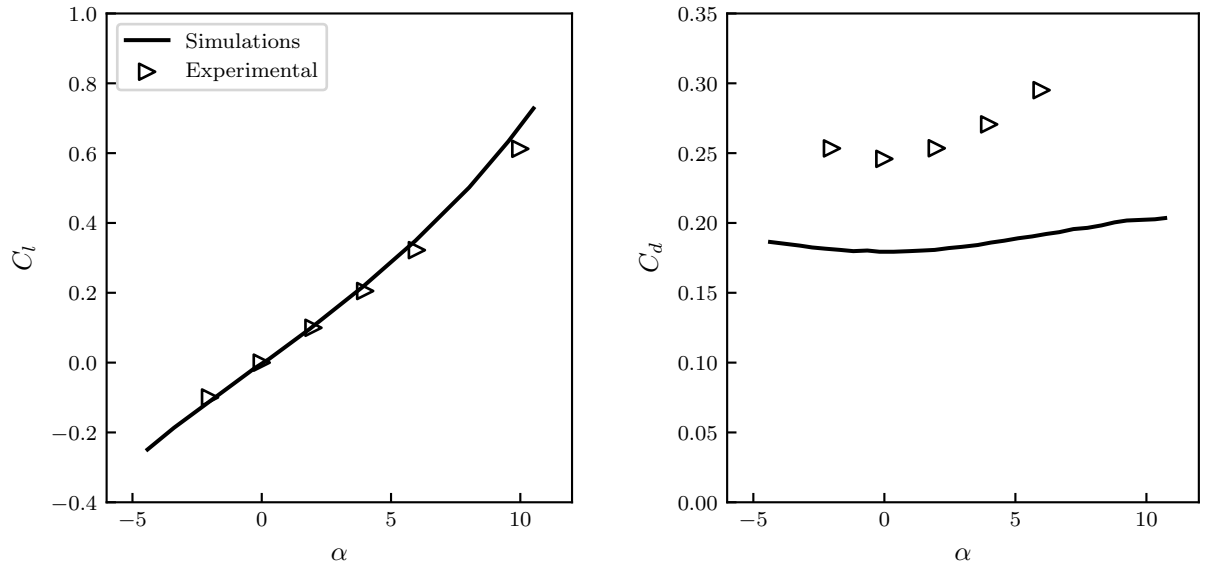

Fig. 4 Case II: Normal (left) and drag force (right) coefficient with various angles of attack [32]. Here we consider the static case (with no spinning) as in the reference.

For the validation of Case II, we also reproduce the experimental results at a fixed angle of attack of $\alpha = 4.2°$ for various non-dimensional spin rates. The computed Magnus force coefficient is shown in figure 5. The Magnus force coefficient is perfectly captured for all experimentally tested non-dimensional spinning rates. These results do highlight the expected low coefficient values compared to the lift or normal force of this same projectile. In the unsteady run, the Magnus force becomes stable after half cycle, therefore, the coefficient that we report here is averaged in the second half.

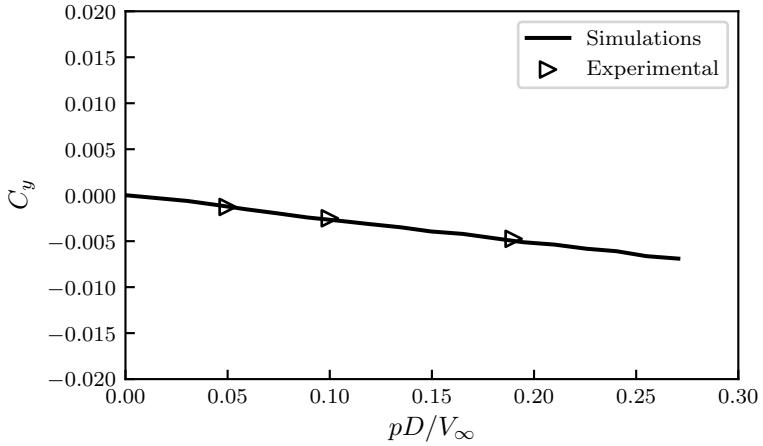

Fig. 5 Case II: Magnus force coefficient at a fixed angle of attack $\alpha = 4.2°$ for varying non-dimensional spinning rate [32].

C. Boundary layer profile validation

The validation of the turbulent boundary layer profile on various projectiles was done by [33]. They measured the velocity profile near the wall at a fixed location of $x/D = 3.33$ on the windside of the projectile. The other parameters of the experiments are noted in table 1. Interested readers are invited to consult [33] for further details. The data include both a non-spinning and spinning case (spinning rate of 0.19), the simulation results compare favourably to the experimental results as shown in figure 6. The spinning boundary layer contains both a axial velocity component, as shown in the figure, but also a azimuthal velocity component (not shown) which means that the boundary layer profile is fully three-dimensional. The non-spinning case is characterized by a standard two-dimensional boundary layer. As the simulation is able to correctly capture both non-spinning and spinning cases, this allows us to gain confidence in the correct prediction of the boundary layer growth on the projectile.

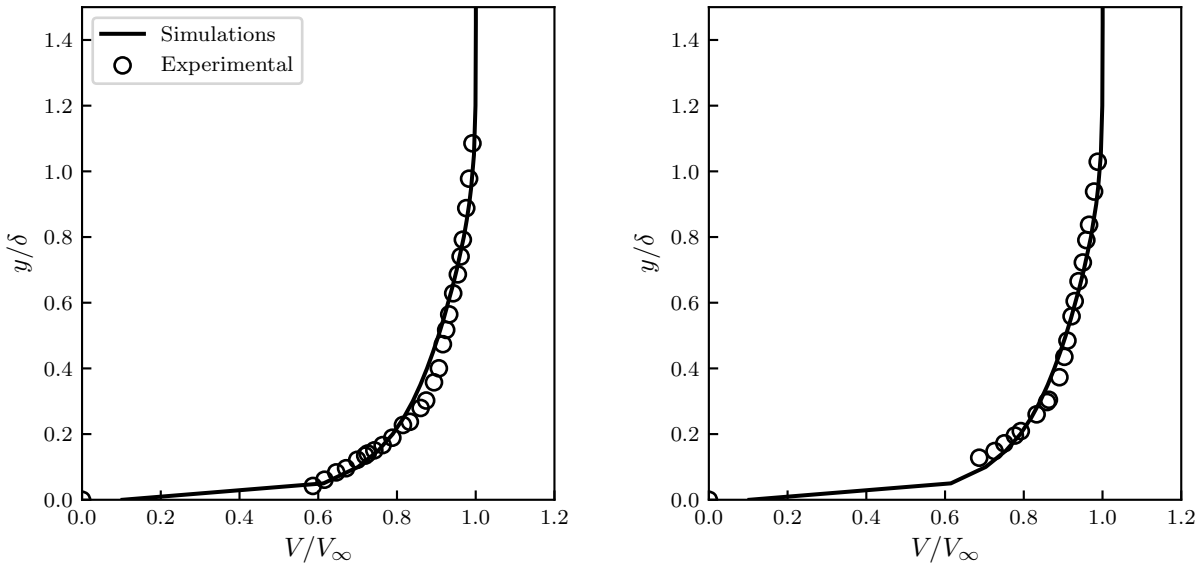

Fig. 6 Case III: The boundary layer profile for the non-spinning (left) and spinning case (right). The experiment was conducted at fixed angle of attack of $\alpha = 4.2°$. The experimental results are from [33].

V. Results and Discussions

The validation cases, presented in the previous section, provide compelling evidence about the accuracy of the computational methods for the Magnus force estimation. By comparing pressure, aerodynamic coefficients, and boundary layer profiles we obtain a reliable baseline simulations that are used to study the parametric effects on the Magnus force computation. In the present section, we investigate the effects of the modelling of the boundary layer on the Magnus force computation of a spin-stabilized projectile. This is undertaken for two main reasons: (1) investigate the physical implications of the boundary layer characteristics on the Magnus force coefficient, and (2) understand the

sensitivities of the numerical modelling assumptions on the Magnus force computation. This last point is particularly important as the majority of the engineering-level computations overlook the non-negligible effects of the boundary layer state on the side force estimation. The present work provides guidance on these numerical modelling assumptions for computational fluid dynamics. In the present section, we first investigate the influence of the transition location on the prediction of the Magnus force. Afterwards, we investigate the impact of the freestream turbulence levels and wall boundary conditions on the aerodynamic coefficients. The transitional modelling of a spin-stabilized is investigated and compared to the local transitional trip. Finally, a comparison of the steady and unsteady solvers for an unfinned spinning projectiles is undertaken.

A. Influence of the boundary layer state on Magnus force

In the canonical case of a rotating cylinder in a laminar crossflow, the location of the transition to turbulence can directly affect the magnitude and orientation of the resulting Magnus force. Under very specific operating regimes with flow separation, this can even result in an inverse Magnus force. This is the result of differing pressure gradients on either side of the cylinder which affect the boundary layer separation. On the retreating side (downstream-moving) of the cylinder the separation is delayed whereas on the advancing side (upstream-moving) it arrives precociously. This non-symmetric separation location, impacts the shear force at the wall this in turn distorts the wake and generates a side force. When the transition to turbulence affects the flow separation, especially if it pushes the transition farther downstream, an inverse Magnus effect can appear [18]. Therefore, it is clear that transition to turbulence can play a central role in the Magnus force estimation.

In spin-stabilized projectiles, flow separation can also impact flow Magnus force but such phenomenon typically only occurs at high angles of attack or at very high spin rates. Although we admit that an inverse Magnus force is likely not able to arise in a rotating projectile (with a much shallower angle between the velocity and the rotation vector), the influence of transition can nonetheless impact the magnitude of this side force. Here, we study the impact of the transition location on the resulting Magnus force. In the present simulations, we impose a strip transition at various streamwise locations on the conical nose in order to characterize the variation of the Magnus force. A constant spin rate of 0.19 imposed for two different attack angles. Figure 7 shows the varying affect of the transition location on the Magnus force. The reader should bear in mind that some of the transitional locations are not physically achievable given the highly unstable crossflow boundary layer on the projectile. Nonetheless, this study provides a good evidence to suggest that a difference of about 14% is noted in the Magnus force coefficient between a fully turbulent case (transition at $x/L = 0$) and delayed transition at $x/L = 0.2$ (for the $\alpha = 10^\circ$ case). In other words, by assuming a fully turbulent boundary layer– as is often in the absence of clear knowledge on the actual transition location– a non-negligible error in the Magnus force estimate can be made. Interestingly, an increasing region of laminar flow (delaying the transition to turbulence) acts to reduce the magnitude of the side force.

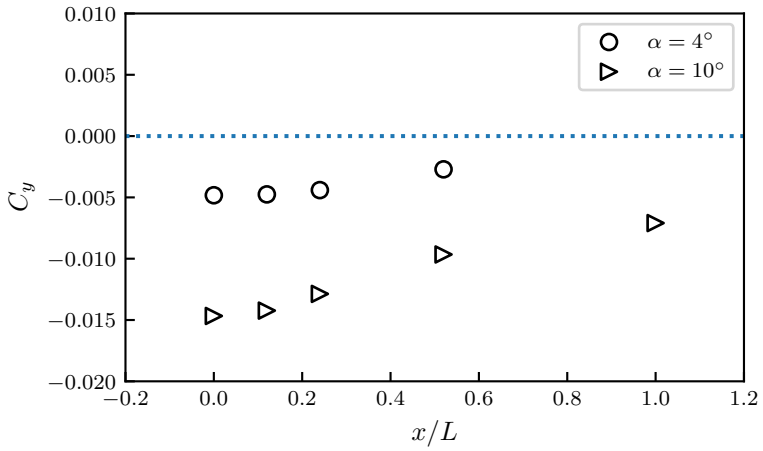

Fig. 7 Impact of transition location on Magnus force coefficient at various angles of attack. The non-dimensional spinning rate is 0.19.

B. Effect of freestream turbulence intensity and boundary conditions

The transition location plays a significant role in determining the evolution of the thickness of the turbulent boundary layer and concomitantly the aerodynamic coefficients. Other modellings assumptions may also play a non-negligible role on the boundary layer development. Two of these modelling assumptions are studied: the level of freestream turbulence and the wall boundary conditions.

In most applied simulations, the freestream turbulence intensity is imposed as an inflow boundary condition to a simulation. The production of turbulent kinetic energy (TKE), P, in standard two-equation Reynolds-averaged Navier-Stokes solver depends on both the mean flow gradients and the eddy-viscosity (which is a function of the TKE):

$$P = \mu_t \frac{\partial \vec{V}}{\partial \mathbf{x}} \tag{7}$$

where μ_t depends on the local value of the TKE among other variables. As a result, the modification of the level of freestream turbulent may directly impact the production of TKE, which in turn can influence the boundary layer development. Figure 8 investigates the influence of the freestream TKE on the Magnus force estimation. For this parametric study, we have a spin rate of 0.19 and an angle of attack of $\alpha = 4.2°$; we impose the transition location at $x/h = 0.72$. Two values of the imposed TKE are studied, namely at 0.3% and 3.3% which correspond to a natural laminar and bypass transition regimes respectively. The influence on the side force estimation for both turbulence intensities remains negligible. Although the reader should bear in mind that the transition location was imposed by a local trip to the boundary and not determined via transitional modelling approximations. By considering the other aerodynamic coefficients and a broader range of angles of attack, as shown in figure 9, we do note a more significant impact of the selected TKE value, especially for the drag coefficient.

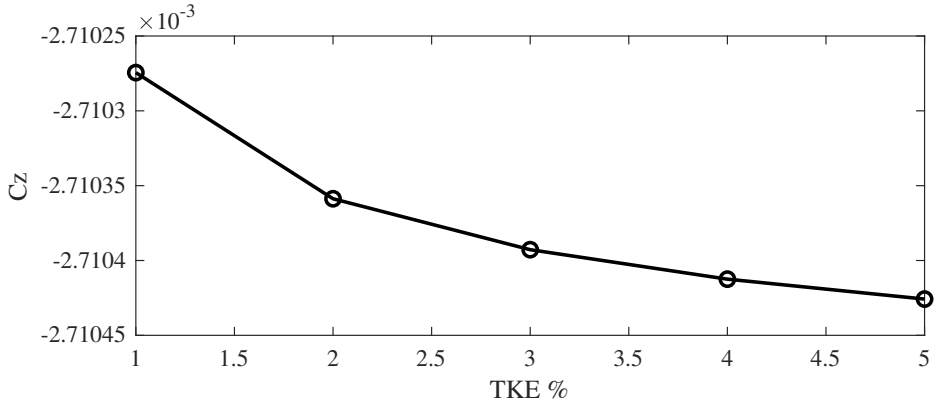

Fig. 8 Impact of the freestream turbulence intensity on the Magnus force. The simulation is run with a trip location at $x/h = 0.72$ for an angle of attack $\alpha = 4.2°$.

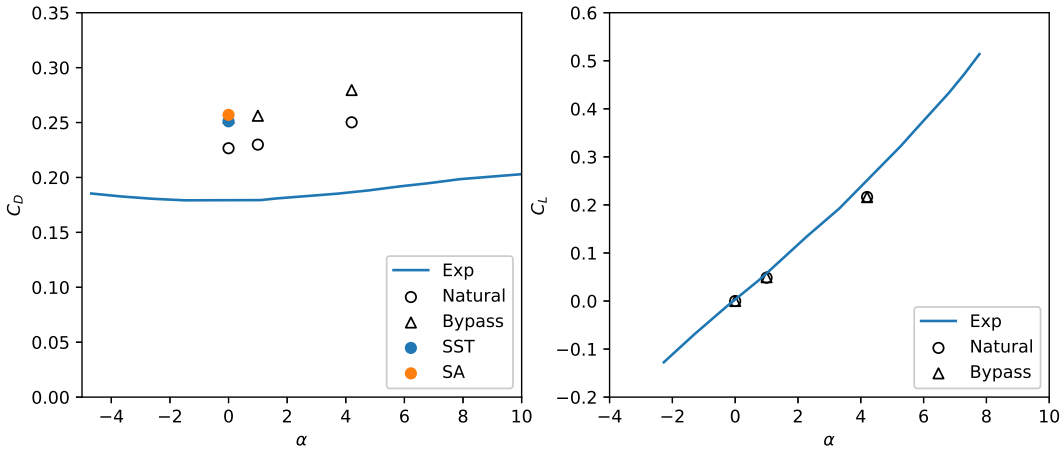

Fig. 9 Influence of the imposed freestream turbulent kinetic energy on the drag (left) and lift (lift) coefficients. The experimental results by Nietubicz *et al.* [32] are shown as comparison. The "natural" and "bypass" transitions correspond to turbulence intensities of 0.3% and 3.3%, respectively.

Whereas the velocity boundary condition of the spinning projectile is unambiguous (non-slip boundary condition), the thermal boundary condition can typically be imposed as an isothermal wall or adiabatic wall. Generally, the thermal boundary condition selection would be motivated by the experiments and/or knowledge about the proposed projectile design. Here, we investigated the impact of the imposed thermal boundary condition on the drag force coefficient at a zero angle of attack in table 2. For the isothermal walls, the temperature is set to the freestream temperature of the simulation. By imposing a fixed transition location ($x/h = 0.722$), the difference in the drag force coefficient is about 6% based on differing thermal boundary conditions. If we do not impose a transition trip but use the four-equation transitional models (as will be further discussed in the next subsection), the difference is only about 3%. For the transition model, the freestream turbulence intensity is set to 0.8% and $\mu_t/\mu_\infty = 50$. It should be noted that there was not significant difference in the Magnus force estimate for all cases.

Table 2 Drag Coefficient at Zero Attack (0.1791 experimentally)

	Fixed Transition	Four Equation Transition Model
Isothermal wall	0.2513	0.2321
Adiabatic wall	0.2371	0.2257

C. Transitional turbulence modelling

As compressibility acts to stabilize the boundary layer and thus delaying transition to turbulence, experimentalists often impose a transition location (by imposing a local boundary layer trip) to avoid the additional challenges and uncertainties associated with transitional flows. From a numerical perspective in two-equation RANS solvers, these trips are imposed in the simulations. Upstream of these physical trips, the turbulence production term (7) is forced to zero; downstream of the trip, the restriction on the production term is loosened and the value of the turbulent kinetic energy evolves following the governing equation. For cases in which the transition location is unknown, we can resort transitional modelling as discussed in section 3. These transitional models, such as the $\gamma - Re_\theta$ model, impose the solution of additional governing equations which can account for the transition to turbulence. These models depend heavily on well-defined correlations to compute the transition. In this subsection, the use of transitional models for the Magnus force estimation on spin-stabilized projectiles is assessed.

To investigate the transition model, two sets of freestream turbulence intensity are intensity are investigated: a natural (freestream turbulence intensity of 0.3%) and bypass (freestream turbulence intensity of 3.3%) transitional regimes are investigated. The freestream value of μ_t/μ also has an impact on the transition location (and surface friction) but are not considered in the present investigation. Figure 10 shows the significant impact of the transition location, and concomitantly on the Magnus force, of the imposed freestream turbulence intensity. The variation of the friction at the wall for the transitional models can be seen in the figure 11. We note that, in contrast to the trip transition, the transitional models do not impose a uniform transition location along the azimuthal direction. This discrepancy means that an inherent difference in the drag force coefficient is expected when compared to the imposed trip transition.

D. Steady or unsteady simulations

As a general rule, the simulation of spin-stabilized devices must be done using an unsteady solver. The rotation can be imparted to the to the projectile by using a moving mesh method or using overset grids (see e.g. [1] for more details). For the specific case of unfinned projectiles, we may also impose the body rotation via the boundary condition. As a result, we can run steady-state simulations with the correct boundary conditions. Here we investigate the impact of the steady computation on the estimate of the Magnus force. For all cases investigated, the difference in the side force estimate was negligible. The computational expense was drastically reduced (about 1 order of magnitude) when computing the steady-state simulations with imposed rotating boundary condition.

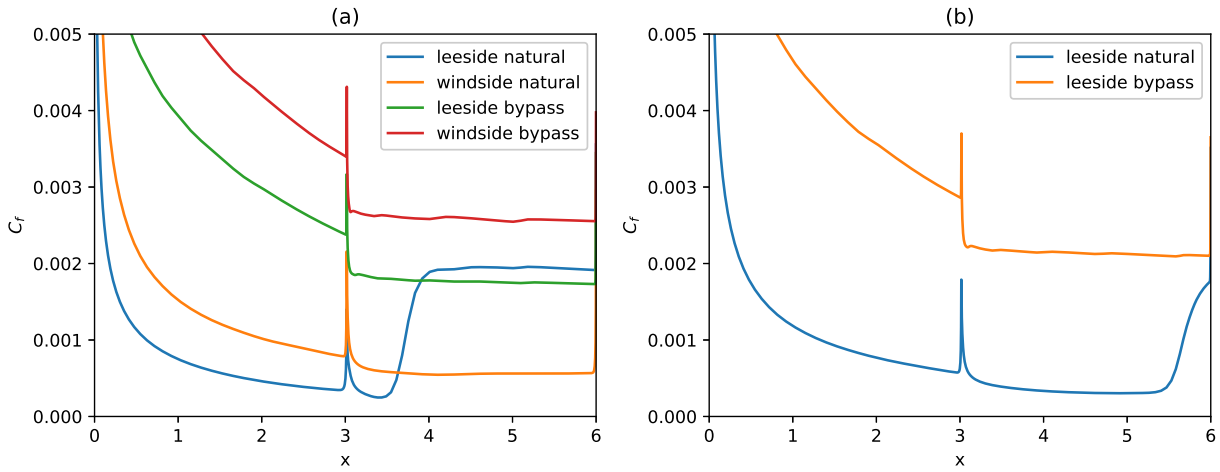

Fig. 10 Surface friction coefficient using the transitional model for the natural (freestream turbulence intensity of 0.3%) and bypass (freestream turbulence intensity of 3.3%) transition simulations.

VI. Conclusion

The Magnus force represents an undamped contribution in spin-stabilized projectiles which is of critical importance for guidance and control. The potential deleterious effects of this highly non-linear force means that an accurate estimation is essential. Furthermore, its relatively small magnitude relative to lift and drag means that it is sensitive to slight fluid dynamic changes particularly with respect to the boundary layer. These modelling of these boundary layer effects are often neglected when estimating the aerodynamic forces on a spin-rotating projectiles using higher-fidelity computational methods in combination with standard engineering-level turbulence closure models. The present work shows the sensitivity of the boundary layer state on the Magnus force estimation for an unfinned rotating projectile. The work highlight the relative sensitivity of a number of the central numerical boundary layer modelling assumptions. A careful validation, with detailed experimental results, is carried out to assure a well-defined baseline case. Thereafter, we conduct a systematic study of the influence of the transition location on the Magnus force estimation which highlights the sensitivity of the force this undamped contribution. We noted a 14% variation in the Magnus force depending if we assume a fully turbulent boundary layer from the leading tip or if we impose a transitional trip slightly downstream on the conical tip (at $x/L = 0.2$). Additionally, we report on the negligible influence of the freestream turbulence intensity and thermal boundary condition for the Magnus force estimation. For the drag force, the impact is more significant (6% variation based on the selection of an adiabatic or isothermal boundary condition, for example). We then investigate of the use of transitional turbulence models in the context of Reynolds Averaged Navier-Stokes which brings to light the more important role of the freestream turbulence intensity on the transition, and concomitantly, the Magnus force estimate. We also note the inherent difficulty of classical transitional models to predict the transition under crossflow conditions. Modifications to transitional models which can account for the premature transition under

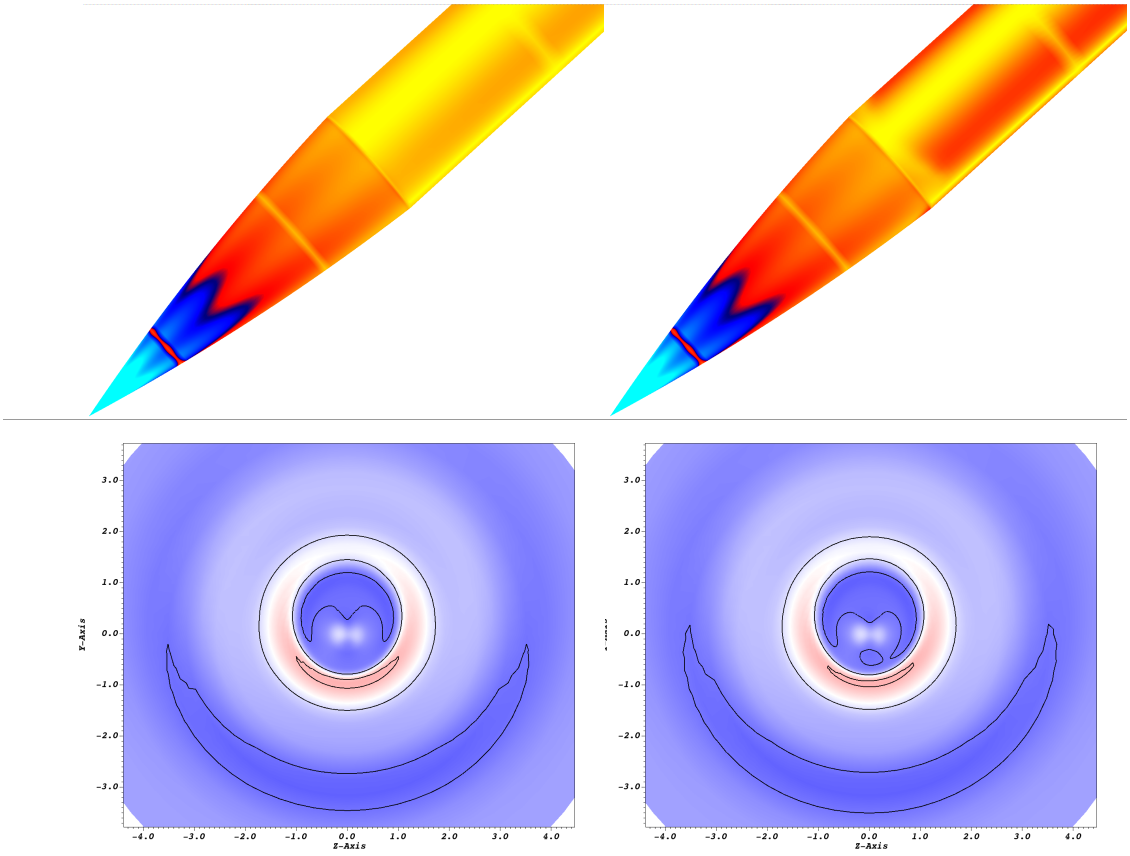

Fig. 11 Qualitative representation of the surface friction for the natural (top left, freestream turbulence intensity of 0.3%) and bypass (top right, freestream turbulence intensity of 3.3%) using the four-equation transitional model. The angle of attack is fixed at $\alpha = 4.2°$. A slice of the pressure distribution in the wake at $x/D = 10$ is shown (bottom) for both cases.

crossflow conditions are deemed more appropriate for the accurate Magnus force estimation of rotating projectiles. Such a study is left for future work.

Funding Sources

Financial support for this work was provided by the Defense Research and Development Canada (DRDC), Valcartier. This research was enabled in part by support provided by SciNet, Sharcnet and Compute Canada (`www.computecanada.ca`).

Acknowledgments

The help and fruitful discussions with Mr. Omar Kamal are acknowledged.

References

[1] Despeyroux, A., Hickey, J.-P., Desaulnier, R., Luciano, R., Piotrowski, M., and Hamel, N., "Numerical analysis of static and dynamic performances of grid fin controlled missiles," *Journal of Spacecraft and Rockets*, Vol. 52, No. 4, 2015, pp. 1236–1252. doi:10.2514/1.A33189, URL http://www.scopus.com/inward/record.url?eid=2-s2.0-84940782553&partnerID=40&md5=6eeb45e5c782d89703f4f1d979a152fa.

[2] Yin, J., Wu, X., Lei, J., Lu, T., and Liu, X., "Canards interference on the Magnus effect of a fin-stabilized spinning missile," *Advances in Mechanical Engineering*, Vol. 10, No. 7, 2018, pp. 1–16. doi:10.1177/1687814018790865.

[3] Fresconi, F., Cooper, G., Celmins, I., DeSpirito, J., and Costello, M., "Flight mechanics of a novel guided spin-stabilized projectile concept," *Proceedings of the Institution of Mechanical Engineers, Part G: Journal of Aerospace Engineering*, Vol. 226, No. 3, 2012, pp. 327–340. doi:10.1177/0954410011408385.

[4] McCoy, R., *Modern Exterior Ballistics The Launch And Flight Dynamics Of Symmetric Projectiles*, 1989.

[5] Oh, S.-y., Kim, S.-c., Lee, D.-k., Kim, S., and Ahn, S.-k., "Magnus and Spin-Damping Measurements of a Spinning Projectile Using Design of Experiments," Vol. 47, No. 6, 2010. doi:10.2514/1.50188.

[6] Sturek, W. B., "1973_BoundaryLayerStudiesOnSpinningBodiesOfRevolution," 1973.

[7] Martin, J., "On Magnus Effects Caused by the Boundary-Layer Displacement Thickness on Bodies of Revolution at Small Angles of Attack," *Journal of the Aeronautical Sciences*, Vol. 24, No. 6, 1957, pp. 421–429. doi:10.2514/8.3872.

[8] Platou, A., "The Magnus force on a finned body," Tech. rep., Ballistic Research Laboratories, 1963.

[9] Leon, H., and Jr, P., "Boundary layer contribution to the Magnus effect on a spinning cylinder at low angles of attack," 1971.

[10] Jacobson, I., "Magnus Characteristics of Arbitrary Rotating Bodies," 1973, p. 66.

[11] Nietubicz, C. J., Sturek, W. B., and Heavey, K. R., "Computations of projectile Magnus effect at transonic velocities," *AIAA journal*, Vol. 23, No. 7, 1985, pp. 998–1004. doi:10.2514/3.9030.

[12] Despirito, J., Silton, S. I., and Ground, A. P., "CAPABILITIES FOR MAGNUS PREDICTION IN SUBSONIC AND TRANSONIC FLIGHT," 2007.

[13] Despirito, J., and Heavey, K. R., "CFD Computation of Magnus Moment and Roll Damping Moment of a Spinning Projectile," *AIAA Atmospheric Flight Mechanics Conference and Exhibit*, 2004, p. 24. doi:doi:10.2514/6.2004-4713.

[14] Cayzac, R., Carette, E., Denis, P., and Guillen, P., "Magnus Effect: Physical Origins and Numerical Prediction," *Journal of Applied Mechanics*, Vol. 78, No. 5, 2011, p. 051005. doi:10.1115/1.4004330.

[15] Doraiswamy, S., and Candler, G. V., "Detached Eddy Simulations and Reynolds-Averaged Navier- Stokes Calculations of a Spinning Projectile," *Journal of Spacecraft and Rockets*, Vol. 45, No. 5, 2008, pp. 935–945. doi:10.2514/1.31935.

[16] Bhagwandin, V. A., "High-Alpha Prediction of Roll Damping and Magnus Stability Coefficients for Finned Projectiles," *Journal of Spacecraft and Rockets*, Vol. 53, No. 4, 2016, pp. 720–729. doi:10.2514/1.A33419, URL http://arc.aiaa.org/doi/10.2514/1.A33419.

[17] Wang, K. C., "Boundary Layer Over Spinning Blunt Body of Revolution at Incidence Including Magnus Forces," *Proceedings of the Royal Society A: Mathematical, Physical and Engineering Sciences*, Vol. 363, No. 1714, 1978, pp. 357–380. doi:10.1098/rspa.1978.0173.

[18] Muto, M., Tsubokura, M., and Oshima, N., "Negative Magnus lift on a rotating sphere at around the critical Reynolds number," *Physics of Fluids*, Vol. 24, No. 1, 2012. doi:10.1063/1.3673571.

[19] Kim, J., Choi, H., Park, H., and Yoo, J. Y., "Inverse Magnus effect on a rotating sphere: When and why," *Journal of Fluid Mechanics*, Vol. 754, 2014, p. R2. doi:10.1017/jfm.2014.428.

[20] Hussain, Z., Garrett, S. J., Stephen, S. O., and Griffiths, P. T., "The centrifugal instability of the boundary-layer flow over a slender rotating cone in an enforced axial free stream," *Journal of Fluid Mechanics*, Vol. 788, 2016, pp. 70–94. doi:10.1017/jfm.2015.671.

[21] Hussain, Z., "Competing instabilities of rotating boundary-layer flows in an axial free-stream," *European Journal of Mechanics, B/Fluids*, Vol. 61, 2017, pp. 316–320. doi:10.1016/j.euromechflu.2016.09.012, URL http://dx.doi.org/10.1016/j.euromechflu.2016.09.012.

[22] Zhang, Q., Wu, X., Yin, J., and Yao, R., "Effect of transition on the aerodynamic characteristics of a spinning cone," *Proceedings of the Institution of Mechanical Engineers, Part G: Journal of Aerospace Engineering*, Vol. 232, No. 11, 2018, pp. 2048–2058. doi:10.1177/0954410017708805.

[23] Siegel, N. W., Schlenker, A. P., Sullivan, K. D., Valdez, I. L., Snow, C. P., Benson, M. J., Van Poppel, B. P., Elkins, C. J., and Rodebaugh, G. P., "An Experimental Setup to Characterize Boundary Layer Asymmetry on a Spinning Projectile Using Magnetic Resonance Velocimetry," 2019, p. V007T09A002. doi:10.1115/imece2018-87472.

[24] Langtry, R. B., and Menter, F. R., "Correlation-based transition modeling for unstructured parallelized computational fluid dynamics codes," *AIAA Journal*, Vol. 47, No. 12, 2009, pp. 2894–2906. doi:10.2514/1.42362.

[25] Grabe, C., and Krumbein, A., "Correlation-Based Transition Transport Modeling for Three-Dimensional Aerodynamic Configurations," *Journal of Aircraft*, Vol. 50, No. 5, 2013, pp. 1533–1539. doi:10.2514/1.C032063, URL http://arc.aiaa.org/doi/abs/10.2514/1.C032063%5Cnhttp://www.scopus.com/inward/record.url?eid=2-s2.0-84888378630&partnerID=tZOtx3y1.

[26] Choi, J. H., and Kwon, O. J., "Enhancement of a Correlation-Based Transition Turbulence Model for Simulating Crossflow Instability," *52nd Aerospace Sciences Meeting*, Vol. 53, No. January, 2014, pp. 1–16. doi:10.2514/6.2014-1133.

[27] Zhou, L., Zhao, R., and Li, R., "A combined criteria-based method for hypersonic three-dimensional boundary layer transition prediction," *Aerospace Science and Technology*, Vol. 73, 2018, pp. 105–117. doi:10.1016/j.ast.2017.12.002, URL https://doi.org/10.1016/j.ast.2017.12.002.

[28] Bartels, R. E., Rumsey, C. L., and Biedron, R. T., "CFL3D Version 6.4 - General Usage and Aeroelastic Analysis," *NASA Technical Memorandum*, , No. April, 2006.

[29] Hanifi, A., and Henningson, D. S., *Stability of Boundary Layer Flows*, Springer Netherlands, Dordrecht, 1999, pp. 51–103. doi:10.1007/978-94-011-4515-2_2, URL https://doi.org/10.1007/978-94-011-4515-2_2.

[30] Langtry, R., and Menter, F., "Correlation-based transition modeling for unstructured parallelized computational fluid dynamics codes," *AIAA Journal*, Vol. 47, No. 12, 2009, pp. 2894–2906.

[31] Reklis, R. P., and Sturek, W., "Surface Pressure Measurements on Slender Bodies at Angle of Attack in Supersonic Flow," Tech. Rep. November, 1978.

[32] Nietubicz, C. J., and Opalka, K., "Supersonic wind tunnel measurements of static and Magnus aerodynamic coefficients for projectile shapes with tangent and secant ogive noses," , No. February, 1980.

[33] Kayser, L. D., and Sturek, W. B., "Experimental measurements in the turbulent boundary layer of a yawed, spinning ogive-cylinder body of revolution at Mach 3.0. Part 1. Description of the experiment and data analysis," Tech. rep., 1978.